Contrib Mineral Petrol (2009) 157:77–93
DOI 10.1007/s00410-008-0321-1

ORIGINAL PAPER

Mechanisms of oxygen isotopic exchange and isotopic evolution of $^{18}O/^{16}O$-depleted periclase zone marbles in the Alta aureole, Utah: insights from ion microprobe analysis of calcite

John R. Bowman · John W. Valley · Noriko T. Kita

Received: 26 January 2008 / Accepted: 20 June 2008 / Published online: 20 August 2008

Abstract Oxygen isotope ratios have been measured by ion microprobe and millimeter-scale dental drill along detailed sampling traverses across the boundary between periclase-bearing ($\delta^{18}O = 11.8‰$) and periclase-free ($\delta^{18}O = 17.2‰$) marble layers in the periclase (Per) zone of the Alta Stock aureole, Utah. These data define a steep, coherent gradient in $\delta^{18}O$ that is displaced a short distance ($\sim$4 cm) into the periclase-free (Cal + Fo) layer. SEM and ion microprobe analyses show two isotopically and texturally distinct types of calcite at the grain scale. Clear (well polished) calcite grains are isotopically homogeneous (within analytical uncertainty; ±0.27‰, 2SD). More poorly polished (pitted), texturally retrograde 'turbid'-looking calcite has lower and more variable $\delta^{18}O$ values, and replaces clear calcite along fractures, cleavage traces or grain boundaries. Despite significant lowering of the $\delta^{18}O$ values in calcite throughout both layers during prograde metamorphism, ion microprobe analyses indicate that individual clear calcite grains are now isotopically homogeneous across the entire gradient in $\delta^{18}O$. Diffusion calculations indicate that conservative time scales required for isotopic homogenization of calcite grains by volume diffusion, 30,000–62,000 years at 575–600°C, exceed significantly the timescale ($\sim$1,250 years) estimated for the prograde development of the $\delta^{18}O$ gradient at the boundary between these two marble layers. The ion microprobe data and these diffusion calculations suggest instead that surface reaction mechanisms accompanying recrystallization are responsible for the observed oxygen isotope homogeneity of these calcite grains. Thus, the ion microprobe data are consistent with the formation of calcite in oxygen isotope exchange equilibrium with infiltrating fluid during prograde reaction and recrystallization.

Communicated by J. Hoefs.

Electronic supplementary material The online version of this article (doi:10.1007/s00410-008-0321-1) contains supplementary material, which is available to authorized users.

J. R. Bowman (✉)
Department of Geology and Geophysics, University of Utah, Salt Lake City, UT 84112, USA
e-mail: bowman@earth.utah.edu

J. W. Valley · N. T. Kita
Department of Geology and Geophysics, University of Wisconsin-Madison, Madison, WI 53706, USA

Introduction

Carbonate rocks subjected to infiltration-driven contact metamorphism often record significant $^{18}O/^{16}O$-depletion due to the infiltration of low $\delta^{18}O$ fluids. However, the mechanisms controlling fluid flow and accompanying isotopic exchange, their rates and the degree to which these processes approach equilibrium, are not well understood, particularly at the grain scale. The recent development of a new generation of ion microprobe with the capacity for high precision (±0.2‰, 2SD) oxygen isotope analyses on $\sim$10 μm diameter spots provides a new tool to test mechanisms of reaction and isotopic exchange on the grain scale, and hence a unique means to evaluate the role of kinetics in these metamorphic processes.

Ion microprobe studies would be particularly useful in evaluating isotopic homogeneity vs. zoning at the grain scale and hence in evaluating the attainment of chemical/isotopic equilibrium at this scale. Such information

provides insights into mechanisms and rates of reaction and isotopic exchange (e.g., diffusion, surface reaction, recrystallization, or a combination) involved in the infiltration-driven metamorphism and $^{18}O/^{16}O$ depletion of carbonate rocks. Several studies have shown that on the mm-, multi-grain scale in metamorphosed carbonates, reaction products are out of exchange equilibrium with reactants (Eppel and Abart 1997; Graham et al. 1998; Matthews et al. 1999; Roselle et al. 1999; Valley 2001; Lackey and Valley 2004; Muller et al. 2004; Pollington et al. 2005). In addition, Wada (1988) and Arita and Wada (1990) have documented oxygen isotope heterogeneity in metamorphic calcite at the grain scale using micro-sampling techniques. Further, a series of theoretical and numerical modeling studies (Lassey and Blattner 1988; Blattner and Lassey 1989; Bowman and Willett 1991; Lasaga and Rye 1993; Bowman et al. 1994; Abart and Sperb 1997; Ague and Rye 1999; Lasaga et al. 2000, 2001; Baumgartner and Valley 2001; Cui et al. 2002, 2003; Bolton et al. 2004; Luttge et al. 2004) point out the potential role of reaction kinetics (reaction overstepping; isotope disequilibrium; development of non-equilibrium steady states) during infiltration-driven decarbonation reactions. Therefore the assumption of exchange equilibrium may not always be justified in modeling isotopic exchange accompanying infiltration-driven reaction. Critical evidence, one way or another, would come from ion microprobe measurement at high precision of the degree of isotopic homogeneity in metamorphic calcite at the grain scale. Ion microprobe studies have documented oxygen isotopic and trace element heterogeneity at the grain scale in metamorphic calcite (Graham et al. 1998; Lewis et al. 1998) and hydrothermally altered feldspar (Cole et al. 2004) and quartz (Valley and Graham 1996). These studies show that ion microprobe analyses, in conjunction with textural studies utilizing SEM and cathodoluminescence (CL) techniques, can document multiple generations of minerals at the grain scale, identify separate fluid flow events and constrain mechanisms of isotopic exchange and transport.

Isotopic exchange on the grain scale may occur by diffusion and/or surface reaction involving processes of dissolution and reprecipitation. Exchange would be facilitated by mass transport of disequilibrium (chemical and isotopic) fluid along grain boundaries and/or fractures involving diffusion or advection, or both. The mechanisms of diffusion and surface reaction should produce quite distinct isotopic profiles within grains (Fig. 1a, b) as these grains proceed to react/exchange—and possibly equilibrate (Fig. 1c)—with the isotopically distinct, infiltrating fluid. The grain size in most metamorphic rocks, particularly marbles, is often >50 μm and is quite sufficient for the new generation ion microprobe with spot sizes of 1–10 μm (Page et al. 2007) to document grain core-to-rim isotope profiles at high precision in order to test these mechanisms.

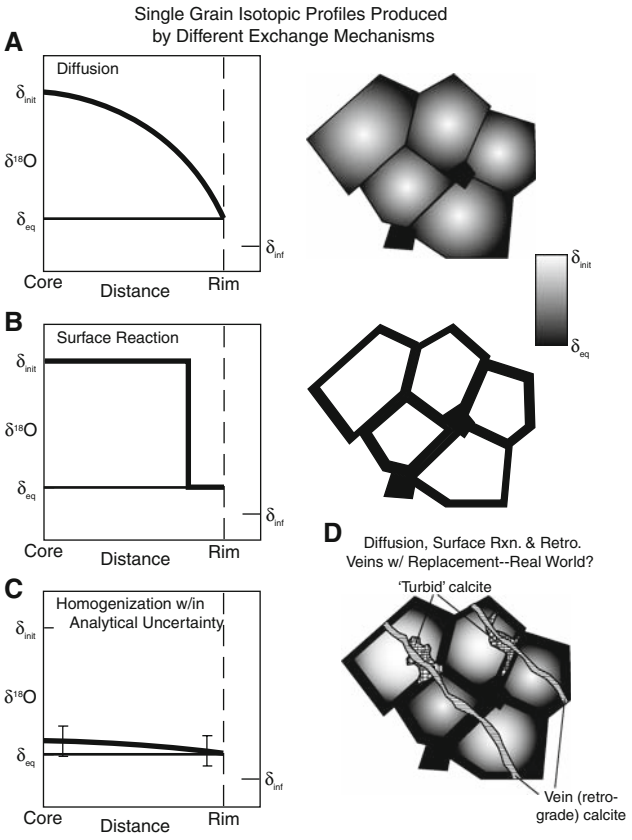

Fig. 1 Schematic $\delta^{18}O$ profiles across a mineral (calcite) grain that would result from different exchange mechanisms between the calcite grain (δ_{init}) and an isotopically distinct grain-boundary fluid (δ_{inf}). **a** Diffusion only; **b** surface reaction (dissolution–reprecipitation) only. Profiles could also be composite, exhibiting effects of both diffusion and surface reaction; **c** attainment of equilibrium (*thin line*, δ_{eq}) to within analytical uncertainty (*heavy line*) as shown with respect to hypothetical error bars; **d** combined effects of diffusion, surface reaction and retrograde vein formation and replacement, but not recrystallization

Micron-scale resolution of the ion microprobe also permits evaluation of the $\delta^{18}O$ values of retrograde features (e.g., alteration rims, alteration along fracture, deformation lamellae and cleavage surfaces) in marbles that can be developed at the sub-mm scale (Valley and Graham 1996; Graham et al. 1998; Lewis et al. 1998; Valley 2001). These different generations commonly have distinct $\delta^{18}O$ values. Conventional sampling techniques at the mm-scale or larger would unavoidably mix these isotopically distinct domains.

In this paper, we report oxygen isotope compositions from a detailed traverse across the boundary between two marble layers at a location (traverse I) in the outer half of the periclase zone of the Alta stock, Utah, contact aureole (Fig. 2). These layers (layers 8 and 9; Fig. 3) appear to be in conformable stratigraphic contact; layer 8 is a calcite (Cal) + forsterite (Fo) marble and layer 9 is a periclase (Per) + Cal + humite group (Hum) marble. Neither layer

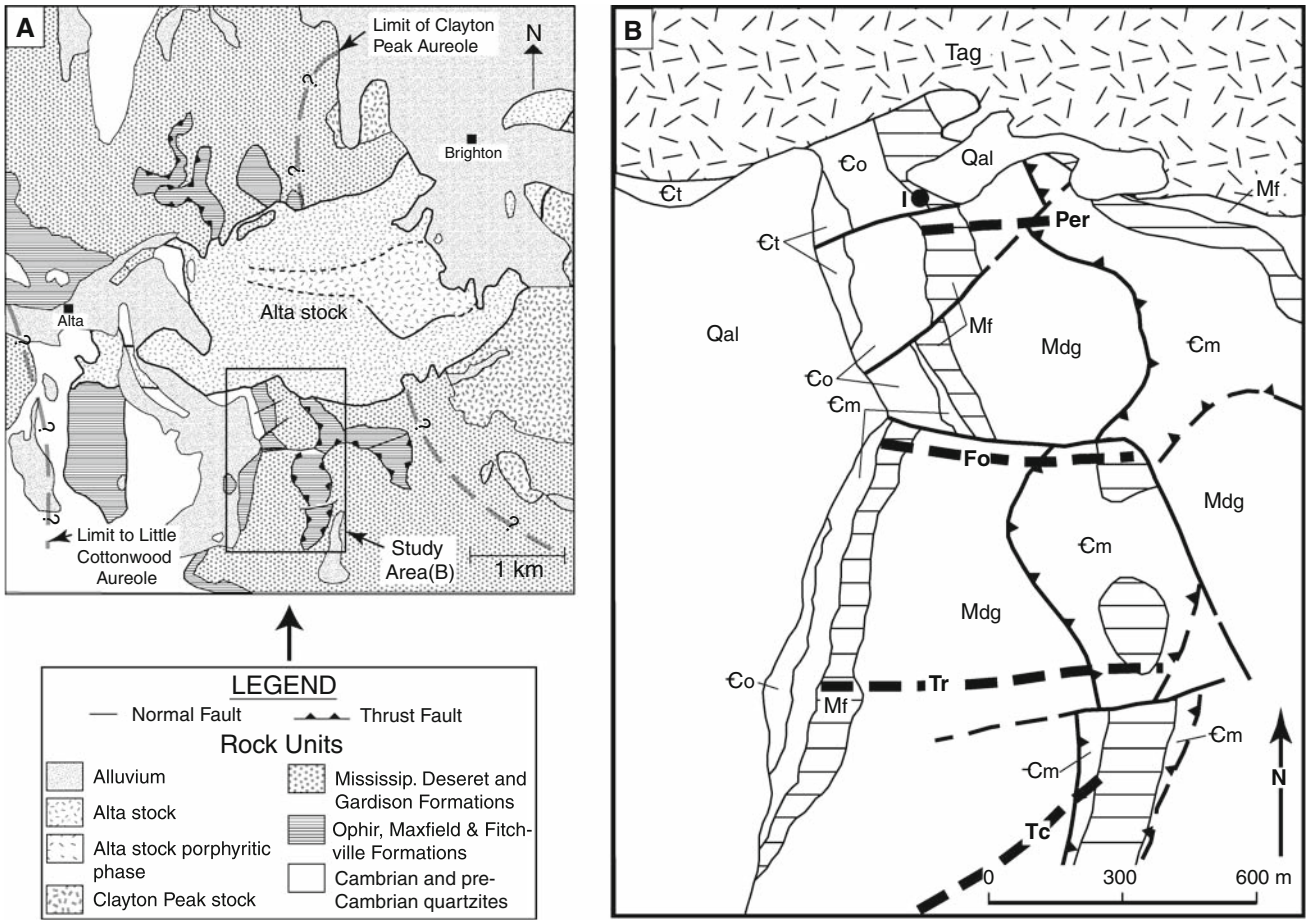

Fig. 2 Geologic map of the Alta stock and contact aureole (**a**) and of the south-central part of the Alta aureole (**b**, study area). Geology after Wilson (1961), Baker et al. (1966) and Cook (1992). Units in (**b**): Ct, Tintic quartzite; Co, Ophir shale; Cm, Maxfield; Mf, Fitchville; Mdg, Deseret and Gardison; Tag, Alta stock granodiorite; Qal, alluvium. In study area **b**, Alta stock shown by random bar pattern; Fitchville (Mf) by the *horizontal line* pattern. The preintrusive Alta-Grizzly thrust (labeled with teeth) has repeated part of the carbonate section, placing the Cambrian Maxfield Formation over the upper Mississippian Deseret-Gardison Formations. Metamorphic isograds (*bold dashed lines*) are after Moore and Kerrick (1976), Cook (1992) and unpublished data, and are labeled by index mineral: *Tc* talc, *Tr* tremolite, *Fo* forsterite, *Per* periclase. In **a**, approximate outer limits of the Little Cottonwood and Clayton Peak aureoles are shown by *heavy dashed lines*. The detailed sample traverse of this study is from area I, 150 m south of the Alta stock (**b**)

contains primary dolomite. The two layers have experienced different fluid fluxes and hence have experienced different extents of $^{18}O/^{16}O$ depletion. The periclase-bearing layer 9 experienced the greater fluid infiltration and has the lower $\delta^{18}O$ value; the two layers differ in $\delta^{18}O$ by 6‰. As a result, a steep gradient in $\delta^{18}O$ is developed at this boundary. This gradient is documented by ion microprobe analyses in thin section and by conventional analyses of samples collected with a 1-mm dental drill. Such isotopic gradients or profiles have been documented at the cm-scale in a number of regional and contact metamorphic terranes. The displacement of these profiles from stratigraphic or structural boundaries and their broadening have been used to constrain timescales of fluid flow, effective diffusivity (D_{eff}) or diffusive lengths in these marble layers with both analytical and numerical models of isotope transport (Ganor et al. 1989; Bickle and Baker 1990a, b; Gerdes et al. 1995; Bickle et al. 1997; Ferry et al. 2001). These models have generally been 1D (with exception of Gerdes et al. 1995) and usually assume equilibrium isotope exchange.

The objectives of this ion microprobe study are to: (1) isolate the oxygen isotope signals of the prograde and retrograde carbonate phases (calcite and dolomite) at this periclase zone site in the Alta aureole; (2) document the degree of isotopic homogeneity at the grain scale in these carbonate minerals which will provide insights into the mechanisms and rates of reaction and isotopic exchange accompanying infiltration-driven reaction in the periclase zone; and (3) define accurately the oxygen isotopic gradient at this boundary. Because fluid flow is dominantly layer-parallel during prograde metamorphism of the periclase zone (Cook et al. 1997), these gradients at layer boundaries are formed on the flanks (sides) of the sheets or

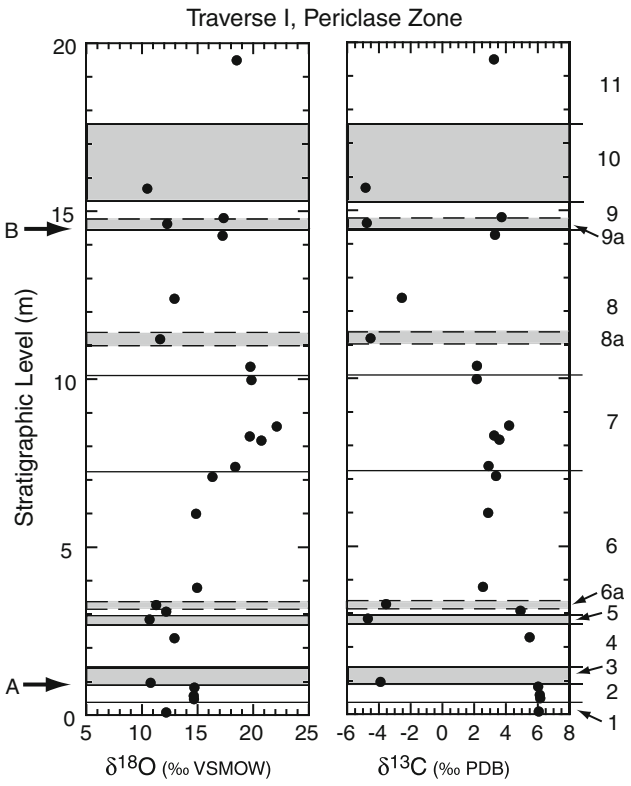

Fig. 3 *Left*: Oxygen isotope compositions ($\delta^{18}O$) of samples from a continuous stratigraphic sequence (traverse I, Fig. 2) of marbles within the Periclase zone in the south Alta aureole (from Cook et al. 1997). Periclase (now brucite)-bearing layers are shown by the *gray pattern*; these are always the lowest $\delta^{18}O$ (<12.5‰) layers. *White layers* are usually forsterite (Fo) + calcite (Cal) marbles. There are significant variations in $\delta^{18}O$ values from one stratigraphic layer to the next; as much as 7‰ difference exists between adjacent beds. Detailed sampling traverses were made across the 2/3 (*arrow labeled* A) and the 8/9 (*arrow labeled* B) boundaries. The traverse across the 8/9 boundary is the focus of this study. *Right*: Carbon isotope compositions ($\delta^{13}C$) in this traverse. In general, $^{13}C/^{12}C$ depletions track $^{18}O/^{16}O$ depletions, and the periclase-bearing layers also have the lowest $\delta^{13}C$ values. Analytical uncertainty for both $\delta^{18}O$ and $\delta^{13}C$ is ±0.1‰

lobes of infiltrating fluid. As such, this gradient is properly defined as an isotopic 'side' (Gerdes and Valley 1994; Yardley and Lloyd 1995). More accurate characterization of such 'sides' will allow future studies to determine with greater confidence what information isotopic 'sides' can or cannot provide concerning parameters and timescales of fluid flow and mechanisms of isotopic transport.

Metamorphic geology of the Alta aureole

The Alta granodiorite stock (38 Ma, Crittenden et al. 1973) has intruded and contact metamorphosed a sequence of Precambrian and Paleozoic quartzites, dolomites, and limestones in the Wasatch Mountains of northern Utah (Fig. 2). Contact metamorphism of siliceous dolomites in the aureole has produced the prograde isograd sequence: talc (Tc), tremolite (Tr), forsterite (Fo), and periclase (Per) toward the igneous contact with the Alta stock (Moore and Kerrick 1976; Cook 1992).

Previous studies have shown that prograde fluid infiltration has driven the breakdown of dolomite to periclase plus calcite to create the periclase zone (Moore and Kerrick 1976; Cook and Bowman 1994, 2000). Applications of calcite (Cal)-dolomite (Dol) geothermometry in the south aureole have defined peak metamorphic temperatures of 575 and 620°C at the periclase isograd and igneous contact, respectively (Cook and Bowman 1994). Stable isotope studies have documented extensive but variable $^{18}O/^{16}O$ depletions in the carbonate wallrocks beneath the pre-intrusive Alta-Grizzly thrust up to 500 m from the igneous contact (Bowman et al. 1994; Cook et al. 1997).

The geothermometry, stable isotope, and petrologic evidence, including calculations of petrologic reaction progress (Cook and Bowman 2000), all indicate that the periclase zone marbles have been infiltrated by significant amounts of water-rich fluids (average total fluid flux, $q_T = 3{,}000\ m^3\ m^{-2}$), and that fluid flow at this level in the aureole was laterally away and down-temperature from the igneous contact in the inner aureole (Bowman et al. 1994; Cook and Bowman 1994, 2000; Cook et al. 1997). Using two-dimensional numerical models of heat and mass (water, oxygen isotopes) transport, Cook et al. (1997) show that a timescale of 5,000 to 6,000 years is sufficient to reproduce simultaneously the temperature (575°C) and observed location of the periclase isograd (max. 200 m from igneous contact) and the observed patterns of large-scale $^{18}O/^{16}O$ depletion in the inner aureole.

Isotopic characteristics of the periclase zone

Prograde fluid infiltration has produced significant but variable $^{18}O/^{16}O$ depletion in these periclase zone marbles (Bowman et al. 1994; Cook et al. 1997). Oxygen isotopic compositions of marble layers have been determined in a measured stratigraphic section, traverse I, in the outer portion of the periclase zone (Fig. 2). Traverse I is located about 150 m from the contact with the Alta stock. Figure 3 shows that there are significant, bed-by-bed variations in $\delta^{18}O$ (and $\delta^{13}C$) values of the marble layers in this section. Individual marble layers in this traverse have been variably depleted in $^{18}O/^{16}O$ because these layers have been subjected to variable fluid flux during prograde metamorphism (Bowman et al. 1994). The $\delta^{18}O$ (Cal) values vary from as high as +22‰ to as low as +10.8‰, compared to original protolith values of >25‰. Isotopic depletions of more than a few per mil are too large to result from devolatilization

effects accompanying the decarbonation reactions occurring in the Alta aureole (Valley 1986). Hence, all layers with $\delta^{18}O < 20‰$ have experienced significant fluid infiltration and $^{18}O/^{16}O$-depletion during contact metamorphism. Layers as thin as 30 cm (e.g., lower part of layer 9) can be isotopically distinct from neighboring layers; adjacent beds are as much as 7‰ different in $\delta^{18}O$ value. The most $^{18}O/^{16}O$-depleted layers (<12.5‰) always contain abundant periclase (now pseudomorphously replaced by brucite) + calcite and lack primary dolomite. Both reaction progress calculations and these maximum $^{18}O/^{16}O$ depletions indicate that the periclase-bearing layers have experienced the greatest fluid flux in Traverse I (Cook and Bowman 2000).

Periclase-bearing marble layers also show petrologic and textural evidence in thin section (secondary dolomite rimming brucite pseudomorphs; dolomite micro-veins) for retrograde reaction and for continued fluid flow during cooling (Cook and Bowman 2000). The stable isotopic impacts of this retrograde fluid flow are at present poorly documented. Calcite grains in the periclase zone typically do not contain visible exsolution lamellae of dolomite in thin section, but the magnesium contents of periclase zone calcite do provide evidence of retrograde reaction during cooling. The maximum temperatures recorded by Cal-Dol geothermometry in samples from the outer half of the periclase zone (vicinity of traverse I) are 540–550°C, lower than maximum temperatures (575°C) recorded farther away near the periclase isograd (Cook and Bowman 1994). Still lower maximum temperatures (~500°C) are recorded by retrogressed calcite near the igneous contact. The good second-order polynomial fit to the Cal–Dol geothermometry results for the entire aureole, excluding these lower retrograded temperatures from the inner periclase zone, defines peak temperatures within the periclase zone to range from 575°C at the periclase isograd up to 625°C at the igneous contact (Cook and Bowman 1994). Numerical modeling of heat and mass transport in the periclase zone (Cook et al. 1997) predicts that Traverse I would cool to below 550°C within ~8,000 years, and to below 500°C within ~20,000 years, following maximum advance of the periclase isograd.

Analytical techniques

Millimeter-scale drill sample traverse, layer 8/9 boundary

The focus of this study is the boundary between layer 8 and the periclase-bearing layer 9 in traverse I (marked with arrow labeled B in Fig. 3). This exposed boundary was sampled and two slabs were sawed at right angle to the boundary. The stratigraphic boundary was identified previously in the field before sampling; the 8/9 boundary was marked on the slab before drilling and isotopic analysis. A dental drill with 0.5 and 1 mm diamond drill bits was used to sample carbonate at intervals as small as 1–2 mm along a continuous, perpendicular 32 cm traverse across the boundary. Oxygen isotopic compositions of calcite were determined using conventional CO_2 gas preparation and mass spectrometry techniques (McCrea 1950) at the University of Utah; analytical uncertainty for both $\delta^{18}O$ and $\delta^{13}C$ is ±0.1‰. Polished thin sections were made from five billets located consecutively along this traverse, from slab material adjacent to the dental drill traverse. Stratigraphic positions of the dental drill holes were marked on these thin sections so that the ion microprobe analyses in these mounts could be located accurately with respect to the dental drill sample analyses.

Ion microprobe ($\delta^{18}O$) analyses

Operating and analytical conditions for the University of Wisconsin CAMECA ims-1280 used in the oxygen isotope analysis of carbonates in this study are described in detail by Kita et al. (2004, 2007) and Page et al. (2007). The Cs^+ primary ion beam (20 keV total acceleration voltage) was focused to a diameter of 10 μm on the sample surface, and the secondary O^- ions were accelerated by −10 kV, and an electron gun was used for charge compensation. The primary ion intensities were ~2 nA. The secondary optics are similar to those in Kita et al. (2007) which achieve high secondary ion transmission. Detailed alignment includes: transfer lens magnification of 200, contrast aperture (CA) 400 μm diameter, field aperture (FA) 4,000 × 4,000 μm square, entrance slit 122 μm width, energy slit 40 eV width, and exit slit width 500 μm. At these conditions, both primary ion spot transferred to FA window and the cross over image through the CA and entrance slit were almost fully transmitted. The mass resolving power (MRP) was ~2,500, sufficient to separate hydride interferences on ^{18}O. Two Faraday cup (FC) detectors were used to simultaneously measure ^{16}O and ^{18}O, equipped with different amplifiers (10^{10} and 10^{11} Ω resistors, respectively). The measured intensity of ^{16}O was ~2×10^9 cps (~10^9 cps/nA). The base line of the FC amplifiers was calibrated once each day; drift during the day was insignificant compared to the noise level of the detectors (≤1,000 cps for the 10^{11} Ω FC). At each analysis position, any small misalignment of the secondary optics was automatically tuned by scanning deflectors before the isotopic measurement started. Total analytical time per spot was about 5 min, including time for locating and selecting the analytical positions, pre-sputtering (10 s), automatic retuning of the secondary ions (~60 s), and analysis (80 s). Data were corrected for the instrumental mass fractionation (IMF) using the UWC-1

calcite ($\delta^{18}O = 23.36$, $\delta^{13}C = -2.03$) standard that was cast and polished in the center of sample mounts within 5 mm of all analyzed grains. The difference in IMF for calcite and dolomite [Δ_{IMF}(Cal–Dol) = 5.5‰] was calibrated by analysis of the UW6220 and UW6250 dolomites and UWC-1 calcite standards in the same mount. Standards were measured four times every 10–20 sample analyses. The IMF correction is based on the average of the standard analyses (normally $N = 8$) bracketing each group of the sample analyses. The external errors of the sets of 8 bracketing standard analyses (on separate spots) are included in eTable 1 of Electronic Supplementary Material and range from 0.15–0.49 (2SD), averaging 0.27‰ (2SD) for 10 μm spot analyses, which represents the spot to spot reproducibility or precision. All sample and standard data are reported in eTable 1 of Electronic Supplementary Material. Oxygen isotope ratios are normalized relative to VSMOW and reported in standard $\delta^{18}O$ notation.

Analytical results

Oxygen isotope profile at the layer 8/9 boundary

Figure 4 is a plot of the $\delta^{18}O$ values of carbonate (calcite) from the mm-scale drill samples across the 8/9 boundary; analyses are compiled in Table 1. The drill sample data define an inflected oxygen isotope gradient between the two layers, which is displaced a short distance (~4 cm) into the underlying layer 8. This gradient in $\delta^{18}O$ is steep and generally coherent, but there is a group of samples near the layer 8/9 boundary (each marked with an 'A') with $\delta^{18}O$ values well below the trend of adjacent analyses. Ion microprobe data and textural observations presented in the next section provide critical evidence that explain these very low $\delta^{18}O$ values. Excepting these apparently anomalous values, the $\delta^{18}O$ values of the interiors of layers 8 and 9 are quite different (averaging 17.2 and 11.8‰, respectively), and exhibit some modest (≤1‰) variation, particularly in layer 9. However, the interiors of both layers 8 and 9 are significantly depleted in $^{18}O/^{16}O$ compared to the unmetamorphosed carbonate protolith ($\delta^{18}O > 25$‰).

Ion microprobe $\delta^{18}O$ results

Ion microprobe analyses of oxygen isotope compositions were made on calcite and dolomite in five polished thin section mounts located within the $\delta^{18}O$ profile across the layer 8/9 boundary. Included in these analyses were detailed ion microprobe traverses across each of these five polished mounts. The results are compiled in eTable 1 of Electronic Supplementary Material.

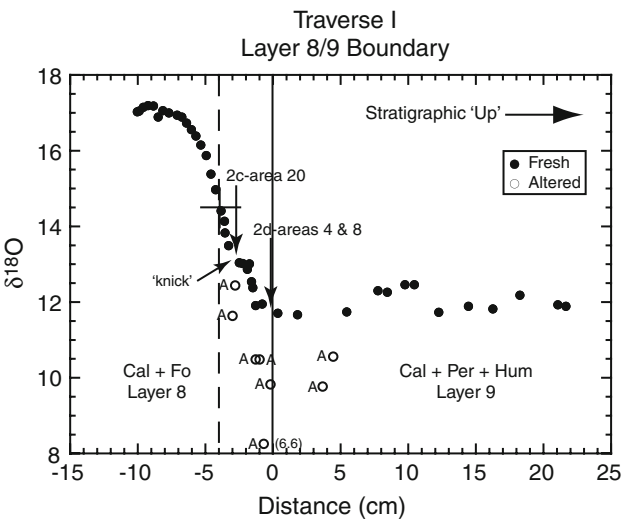

Fig. 4 Plot of the variation in $\delta^{18}O$ values of carbonate versus stratigraphic level across the boundary defined petrographically in thin section between layer 8—a calcite (Cal) + forsterite (Fo) marble and layer 9—a periclase (Per) + Cal + humite group (Hum) marble—from Traverse I (Figs. 2, 3). The oxygen isotope profile is defined by drill data as discussed in the text. Analytical uncertainty for $\delta^{18}O$ (±0.1‰) corresponds to the diameter of the *sample circles*. In general, the drill data define a steep, coherent gradient in $\delta^{18}O$ that is displaced a short distance (4 cm) to the left of (*below*) the 8/9 boundary, as indicated by the midpoint (marked with *cross* and *dashed line* at −4cm) of the gradient. Location in this $\delta^{18}O$ profile labeled 'knick' discussed in text. Samples labeled with 'A' have anomalously low $\delta^{18}O$ values compared to their close neighbors and to the overall profile. The locations of three sites (mount 2c-area 20; mount 2d-areas 4 and 8) investigated with in situ ion microprobe analysis of $\delta^{18}O$ are shown with *two arrows*. Ion microprobe data and textures from these sites (presented in Fig. 5) suggest that these eight drill samples with anomalously low $\delta^{18}O$ values are altered and depleted in $^{18}O/^{16}O$ during retrograde evolution of these marbles

Oxygen isotope distinction between prograde and retrograde calcite

In Fig. 5, ion microprobe data are superimposed on SEM images from four locations in traverse I. Three of these sites (Fig. 5a–c) are located within the $\delta^{18}O$ profile at the layer 8/9 boundary near drill samples with anomalously low $\delta^{18}O$ values (Fig. 4). The SEM images and the ion microprobe data show that there are two isotopically and texturally distinct types of calcite at the grain scale in these locations. Clear (well polished) calcite grains are isotopically homogeneous (within analytical uncertainty; ±0.15 to 0.49‰, 2SD) and have $\delta^{18}O$ values equal to or near those of the main trend defined by the drill samples in layer 8 at this location (Fig. 5a, area 2c-20) or to those defined by most of the drill hole data within layer 9 (Fig. 5b, c; areas 2d-4 and 8). Areas of much less well-polished, pitted, and 'turbid'-looking calcite are developed as thin pitted traces associated with fractures and along cleavage traces within individual grains (Fig. 5a, area 2c-20), next to retrograde dolomite veins

Table 1 Compilation of the $\delta^{18}O$ and $\delta^{13}C$ values of calcite from dental drill samples taken on a traverse across the layer 8/9 boundary in traverse I from the periclase zone of the Alta aureole

Sample	Distance (cm)[a]	$\delta^{18}O$ (SMOW)[b]	$\delta^{13}C$ (PDB)	Sample	Distance (cm)[a]	$\delta^{18}O$ (SMOW)[b]	$\delta^{13}C$ (PDB)
9-2-a-1	18.2	12.20	–4.82	9-2-b-12	–5.75	16.41	3.27
9-2-a-2	14.4	11.91	–4.76	9-2-b-13	–6.1	16.58	3.29
9-2-a-3	10.4	12.48	–4.76	9-2-b-14	–6.45	16.75	3.29
9-2-a-4	9.7	12.48	–4.69	9-2-b-15	–6.8	16.91	3.23
9-2-a-5	4.4	10.58[A]	–4.56	9-2-b-16	–7.15	16.96	3.20
9-2-a-6	21.6	11.91	–4.83	9-2-b-17	–7.75	17.02	3.23
9-2-a-7	21.0	11.95	–4.88	9-2-b-18	–8.2	17.08	3.24
9-2-a-8	8.4	12.28	–4.73	9-2-b-19	–8.55	16.91	3.23
9-2-a-9	7.7	12.32	-4.71	9-2-b-20	–8.9	17.20	3.21
9-2-a-10	5.4	11.76	–4.62	9-2-b-21	–9.3	17.21	3.23
9-2-a-11	–10.1	17.05	3.27	9-2-b-22	–9.65	17.17	3.25
9-2-a-12	–3.9	14.43	2.18	9-2-b-23	–9.95	17.07	3.25
9-2-a-13	–1.65	12.56	–2.33	9-2-c-1	–1.8	13.03	–0.92
9-2-a-14	–1.55	12.40	–2.70	9-2-c-2	–1.35	11.93	–2.44
9-2-b-1	–1.95	12.89	–1.85	9-2-c-3	–1.35	10.51[A]	–2.49
9-2-b-2	–2.3	13.04	–2.42	9-2-c-4	0.3	11.73	–3.44
9-2-b-3	–2.55	13.06	–2.50	9-2-c-5	1.75	11.69	–4.42
9-2-b-4	–2.85	12.46[A]	–2.06	9-2-c-6	–1.05	10.51[A]	–2.49
9-2-b-5	–3.05	11.66[A]	–1.72	9-2-c-7	–0.7	6.58[A]	–2.57
9-2-b-6	–3.35	13.51	–1.14	9-2-c-8	−0.25	9.85[A]	−2.73
9-2-b-7	−3.65	14.16	0.16	9-2-c-9	3.65	9.77[A]	−4.54
9-2-b-8	−4.3	14.99	2.70	9-2-c-10	−3.6	13.85	−1.45
9-2-b-9	−4.65	15.40	3.01	9-2-c-11	−0.85	11.97	−3.19
9-2-b-10	−5.0	15.89	3.14	9-2-c-12	12.2	11.75	−4.76
9-2-b-11	−5.4	16.17	3.19	9-2-c-13	16.2	11.84	−4.75

[a] Distance measured above (+) or below (−) the stratigraphic boundary between layers 8 and 9

[b] Anomalously low $\delta^{18}O$ data marked with superscript 'A' in this table and in Fig. 4

(Fig. 5c, d; areas 2d-8 and 3-2a) and replacing whole grains of calcite (Fig. 5b, area 2d-4). The ion microprobe data indicate that this 'turbid' calcite has significantly lower and more variable $\delta^{18}O$ values than clear calcite (Fig. 5), and the textural relationships illustrated in the SEM images indicate that turbid calcite replaces earlier formed clear calcite. Retrograde dolomite veins in these samples also have significantly lower and more variable $\delta^{18}O$ values than clear calcite (eTable 1; Fig. 5). Turbid calcite grains typically contain small blebs of dolomite (Fig. 5b). These blebs of dolomite likely either precipitated from the retrograde fluids or exsolved from the clear (primary) calcite during its replacement by turbid calcite.

Dental drill samples that contain substantial amounts of this $^{18}O/^{16}O$-depleted 'turbid' calcite have anomalously low $\delta^{18}O$ values that fall below the main profile. A retrograde dolomite vein sufficiently large to be sampled by drill in another layer in traverse I and the 'turbid' calcite adjacent to this vein also have anomalously low $\delta^{18}O$ values (unpublished data). On this basis, we interpret the anomalously low $\delta^{18}O$ values of eight drill samples along the 8/9 traverse to be the result of contribution of $^{18}O/^{16}O$-depleted 'turbid' calcite (marked with an A in Fig. 4). These altered samples are not considered in subsequent discussion. The presence of sub-grain scale 'turbid' calcite may also be responsible for more subtle perturbations in other parts of the $\delta^{18}O$ profile at the 8/9 boundary; for example, the 'knick' in the otherwise smooth $\delta^{18}O$ gradient at −2 to −3 cm below the 8/9 boundary (located near ion microprobe location 2c-area 20, shown by arrow, Fig. 4). This is verified in a later section, where the ion microprobe data traverses within each mount are compared to the drill sample traverse.

Ion microprobe traverse of the layer 8/9 boundary

Ion microprobe analyses were made on clear calcite grains along traverses across each polished mount. In Fig. 6, the $\delta^{18}O$ values of clear calcite grains are plotted as a function of distance (cm) above (+) or below (−) the layer 8/9 boundary. For grains with more than one analysis, the

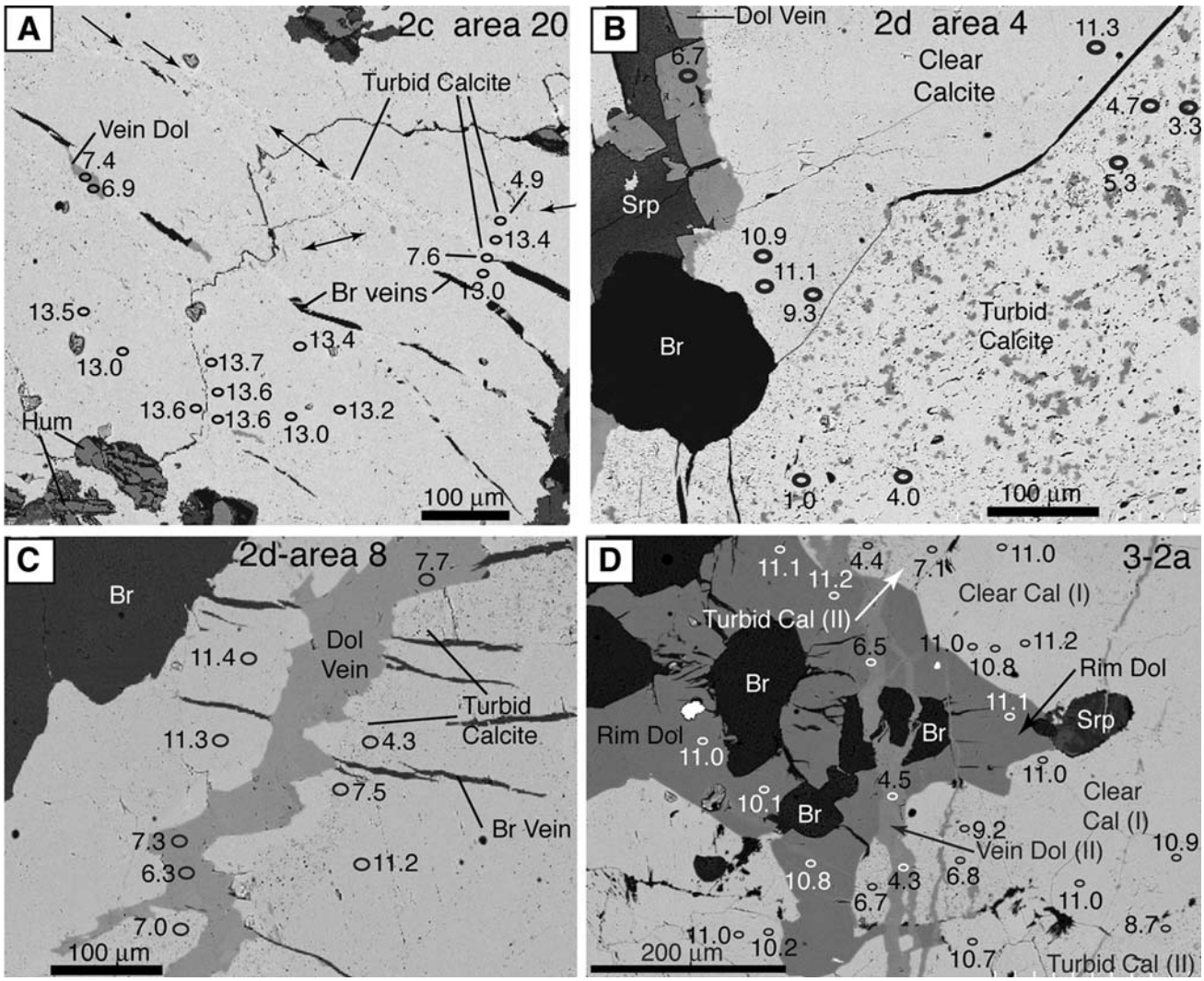

Fig. 5 Back-scattered electron (BSE) SEM images and ion microprobe analyses define two distinct types of calcite—an earlier clear calcite and a later, lower $\delta^{18}O$ 'turbid' calcite—intermixed on a small scale in Traverse I. Area 20 (mount 2c) and areas 4 and 8 (mount 2d) are located within the $\delta^{18}O$ profile at the layer 8/9 boundary (locations shown by *arrows* in Fig. 4); mount 3-2a is from layer 3, traverse I (Fig. 3). **a** (Mount 2c, area 20): *Thin bands* of poorly polished, pitted, and 'turbid'-looking calcite are developed along fractures, cleavage traces and on extensions of brucite (Br)-filled fractures within well-polished, clear calcite. Many of these bands trend from *upper left* to *lower right* in the image, have a slightly lighter BSE *grayscale* than the clear calcite, and occasionally contain small blebs of retrograde dolomite (*darker gray* BSE). *Arrows* mark the traces of some of these *thin bands*. This 'turbid' calcite is significantly depleted in $^{18}O/^{16}O$ compared to the clear calcite. **b** (Mount 2d, area 4): Whole-sale replacement of a calcite grain by 'turbid' calcite (*lower*) and replacement of the edge of an adjacent, clear calcite grain by 'turbid' calcite (*left-center*). Turbid calcite typically contains small blebs of dolomite (*light gray*). **c** (Mount 2d, area 8): Retrograde, low $\delta^{18}O$ dolomite (Dol) vein cross-cutting a clear calcite grain with a selvage of low $\delta^{18}O$ 'turbid' calcite replacing the clear calcite next to this vein. **d** Mount 3-2a: Retrograde, low $\delta^{18}O$ dolomite vein (Dol II) cross-cutting clear calcite grains and an earlier generation of dolomite (Dol I) rimming brucite. The retrograde Dol II vein has a lighter BSE grayscale than the rimming dolomite (Dol I). Turbid, low $\delta^{18}O$ calcite replaces clear calcite near this late dolomite vein. The rim dolomite is retrograde, forming by back-reaction of periclase and calcite prior to hydration of periclase to brucite. However, this early retrograde dolomite is in oxygen isotope exchange equilibrium with the clear calcite

average value for $\delta^{18}O$ and position are plotted. Error bars representing analytical uncertainty (varying from ±0.15 to 0.49‰, 2SD) are attached to each result.

In mount 2a, the measured $\delta^{18}O$ values range from 17.0 to 18.3‰, averaging 17.7‰, but the standard deviation (2SD) of the results from the 25 locations analyzed in mount 2a is ±0.52‰. Hence with two exceptions, the ion probe $\delta^{18}O$ values are constant within analytical uncertainty across the ~1.5 cm traverse analyzed in mount 2a. The ion probe data in mounts 2b and 2c define a coherent trend of systematically decreasing $\delta^{18}O$ toward the layer 8/9 boundary, with one outlier in mount 2b. The decrease

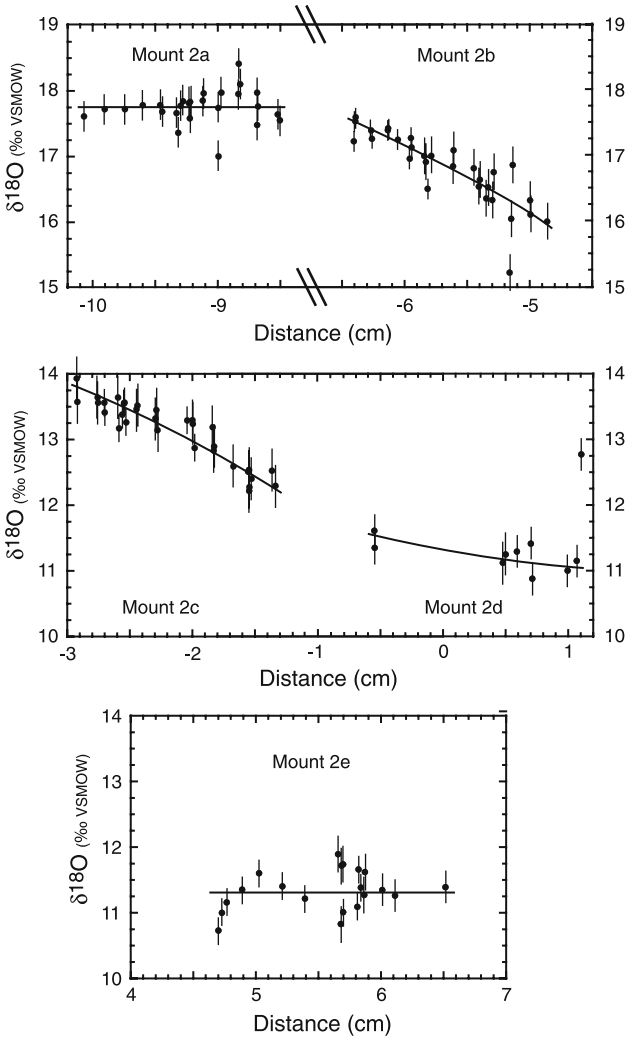

Fig. 6 Plot of ion microprobe $\delta^{18}O$ data for clear calcite grains from mounts 2a–2e as a function of distance (cm) below (−) or above (+) the layer 8/9 boundary. Note that the distance axis is not continuous. *Error bars* representing analytical uncertainty (varying from ±0.15 to 0.49‰, 2SD) are attached to each result. For grains with more than one analysis, the average value for $\delta^{18}O$ and position are plotted. *Lines* have been visually fit to the data from each mount to guide the eye in seeing any trends in the data

in $\delta^{18}O$ across the ~1.5 cm stratigraphic interval of each mount is ~1.6‰, well beyond analytical uncertainty.

Mounts 2d and 2e are located within the uppermost 1 cm of layer 8 and the interior of layer 9, respectively. In mount 2d, nine of the ten analyses are within analytical uncertainty; almost all of the 2‰ range in measured $\delta^{18}O$ values in mount 2d is the result of one high $\delta^{18}O$ (12.8‰) analysis. Although there is a smaller range (1.1‰) in measured $\delta^{18}O$ values in mount 2e, a number of analyses differ by more than the analytical uncertainty of the ion microprobe measurements. Despite this significant variation in $\delta^{18}O$ value, there is no systematic spatial variation in the ion microprobe results within mount 2e.

Comparison of ion microprobe and drill sample $\delta^{18}O$ data across the layer 8/9 boundary gradient

The ion microprobe analyses of clear calcite measured in the five polished mounts (solid diamonds) are superimposed on the $\delta^{18}O$ profile defined by the dental drill samples (open circles) in Fig. 7. Although the ion microprobe results confirm the basic geometry and location of the profile defined by the drill samples, there are some systematic differences. Within mount 2c, the ion microprobe data duplicate exactly the drill sample data at the top of 2c (1–1.5 cm below the 8/9 boundary) and define a systematic gradient of increasing $\delta^{18}O$ values to 2.9 cm below the 8/9 boundary. The ion microprobe data vary systematically across the interval from −2 to −3.5 cm, straightening out the 'kink' recorded in the drill sample data. It is likely that the drill sample data in this interval contain modest amounts of the low $\delta^{18}O$ 'turbid' calcite. Petrographic inspection of this mount confirms the presence of turbid calcite along fractures and cleavage planes within otherwise clear calcite grains. Within mount 2b, the ion microprobe data match exactly the $\delta^{18}O$ values of the drill sample data at the top of the mount (−4.6 cm), but ion microprobe $\delta^{18}O$ values increase to as much as 0.7‰ higher than the $\delta^{18}O$ values defined by the drill data at the bottom of the mount (−6.3 cm). Within mount 2a (interior of layer 8, 8 to 10 cm below the 8/9 boundary), the ion microprobe data are homogeneous in $\delta^{18}O$ within analytical uncertainty and average 17.6‰ (see previous section). The $\delta^{18}O$ values of drill samples from this same stratigraphic interval are also homogeneous but average 17.1‰, 0.5‰ lower than the ion microprobe data (Fig. 7). As a result, the ion microprobe data from mounts 2a and 2b define a higher and sharper 'shoulder' to the $\delta^{18}O$ profile at the layer 8/9 boundary. These differences between ion microprobe and drill data in mounts 2a and 2b suggest the presence of a lower $\delta^{18}O$ component in the drill samples from this section of layer 8. Turbid calcite has not been observed in either mount 2a or 2b, suggesting that this low $\delta^{18}O$ component resides on grain boundaries.

Ion microprobe data in both mounts 2d and 2e are somewhat lower (≤1‰) than the equivalent drill data, indicating that there is a higher $\delta^{18}O$ component in most of the drill samples from layer 9. This higher $\delta^{18}O$ component is either an early retrograde component of calcite preceding or accompanying hydration of periclase to brucite, or layer 9 was not uniformly (to <1‰ variation) depleted in $^{18}O/^{16}O$ during prograde infiltration because of cm-scale heterogeneities in fluid flux. Limited ion microprobe data suggest that both components may be present. One grain of clear calcite analyzed by ion microprobe at approx. +1.2 cm above the 8/9 boundary has a significantly higher $\delta^{18}O$ value of 12.8 (Fig. 7). This appears to be a good

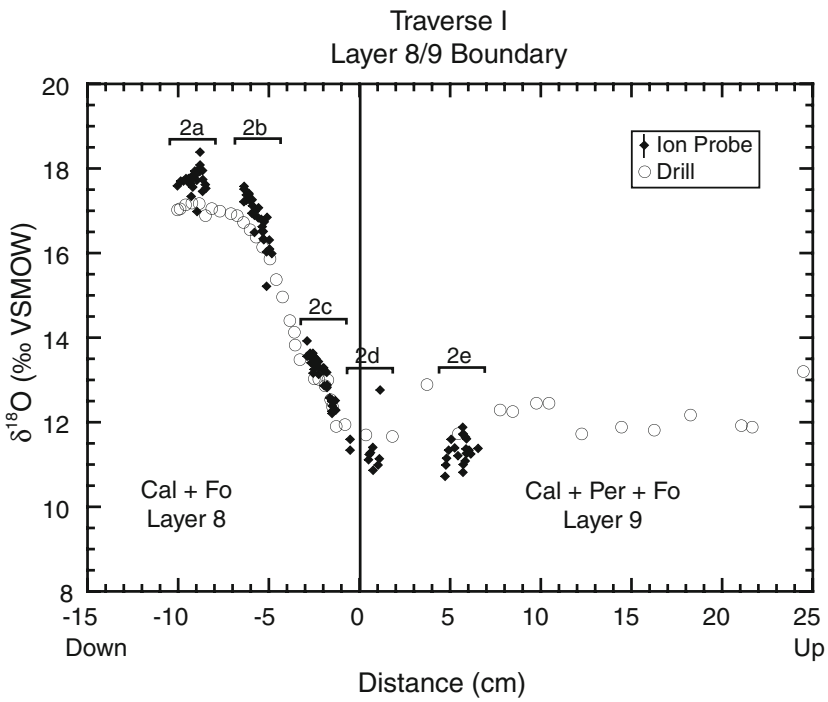

Fig. 7 Comparison of the oxygen isotope profile at the layer 8/9 boundary defined by ion microprobe data (*solid diamonds*) with that defined by the dental drill data (*open circles*) from Fig. 4. Analytical uncertainty for the drill data (±0.1‰) is about two-thirds the diameter of the *sample circles*. Analytical uncertainty for the ion microprobe data averages ±0.27‰, which is shown by an *error bar* attached to the *diamond symbol* in the legend. *Solid lines* labeled with mount numbers show stratigraphic intervals covered by the five polished thin section mounts in which ion microprobe $\delta^{18}O$ analyses were measured

analysis (analytical precision of ±0.25‰, 2SD) and may reflect a somewhat less $^{18}O/^{16}O$-depleted primary domain in layer 9. Additionally, one ion microprobe analysis from mount 2e (area 5, Fig. 8e; see next section) documents the presence of $^{18}O/^{16}O$-enriched 'turbid' calcite in the interior of an otherwise clear calcite grain; this type of 'turbid' calcite is closely associated with brucite-filled fractures and hence with early retrograde fluids.

Oxygen isotope characteristics at the grain scale (intra-grain $\delta^{18}O$ homogeneity)

One of the remarkable characteristics of the ion microprobe data from the 8/9 boundary traverse is that clear calcite grains are isotopically homogeneous, within analytical uncertainty, across the entire gradient in $\delta^{18}O$, not just within the relatively homogeneous interiors of layers 8 and 9. Figure 8 shows SEM images, superimposed with pit locations and the $\delta^{18}O$ values measured by the ion microprobe, from six different locations along the 8/9 boundary gradient where multiple analyses were made of individual clear calcite grains. In addition, multiple analyses were made on single grains at two locations (2d-area 4, 2d-area 8) illustrated in Fig. 5. Although the density of data is less from the sites in mounts 2d and 2e (layer 9), the available data show that the clear calcite domains within individual grains in both of these mounts are without exception isotopically homogeneous, within analytical uncertainty. There is no evidence for isotopic gradients or step functions (e.g., $^{18}O/^{16}O$-depleted grain margins) not only within grains from the relatively homogeneous interiors of layers 8 and 9, but also in grains within the boundary gradient (mounts 2b and 2c).

Comparison of numerous measurements of clear calcite grain interiors to grain margins across the layer 8/9 boundary (Fig. 9) emphasizes that the clear calcite grains are typically homogeneous in $\delta^{18}O$ value. At any position along the $\delta^{18}O$ profile, average $\delta^{18}O$ values of grain interiors and margins are very similar, and total variation in $\delta^{18}O$ values of interiors and margins is small, as shown by low values of standard deviations for the populations at each location (Fig. 9). That is, the variability of $\delta^{18}O$ values within any one mount (or half-mount in the cases of mounts 2b and 2c)—as indicated by the standard deviation of that population of analyses—is usually not much greater than the analytical uncertainty of individual data points. For example, the variability of 21 grain margin analyses in mount 2a (±0.48, 2SD) is only slightly greater than the analytical uncertainty (±0.27, 2SD) of the individual analyses in this mount (Fig. 9). The small variability (low SD) of the analyses within each mount (or half-mount) also indicates that grain-to-grain variability in $\delta^{18}O$ value is small at any one location along this traverse.

Isotopically homogeneous grains, within analytical uncertainty, are in fact compatible (e.g., equilibrated) with the $\delta^{18}O$ gradient recorded by both drill sample and ion microprobe data within the 8/9 boundary profile. This is because the scale of the gradient in $\delta^{18}O$ at the 8/9 boundary (~7 cm width) is much greater than the scale of individual calcite grains. The slope of this $\delta^{18}O$ gradient is ~5.5‰ per 7 cm or ~0.08‰/mm. Although there are calcite grains as large as 2–5 mm in diameter within layer 8, typical grain size is ~1 mm or less within the stratigraphic interval containing

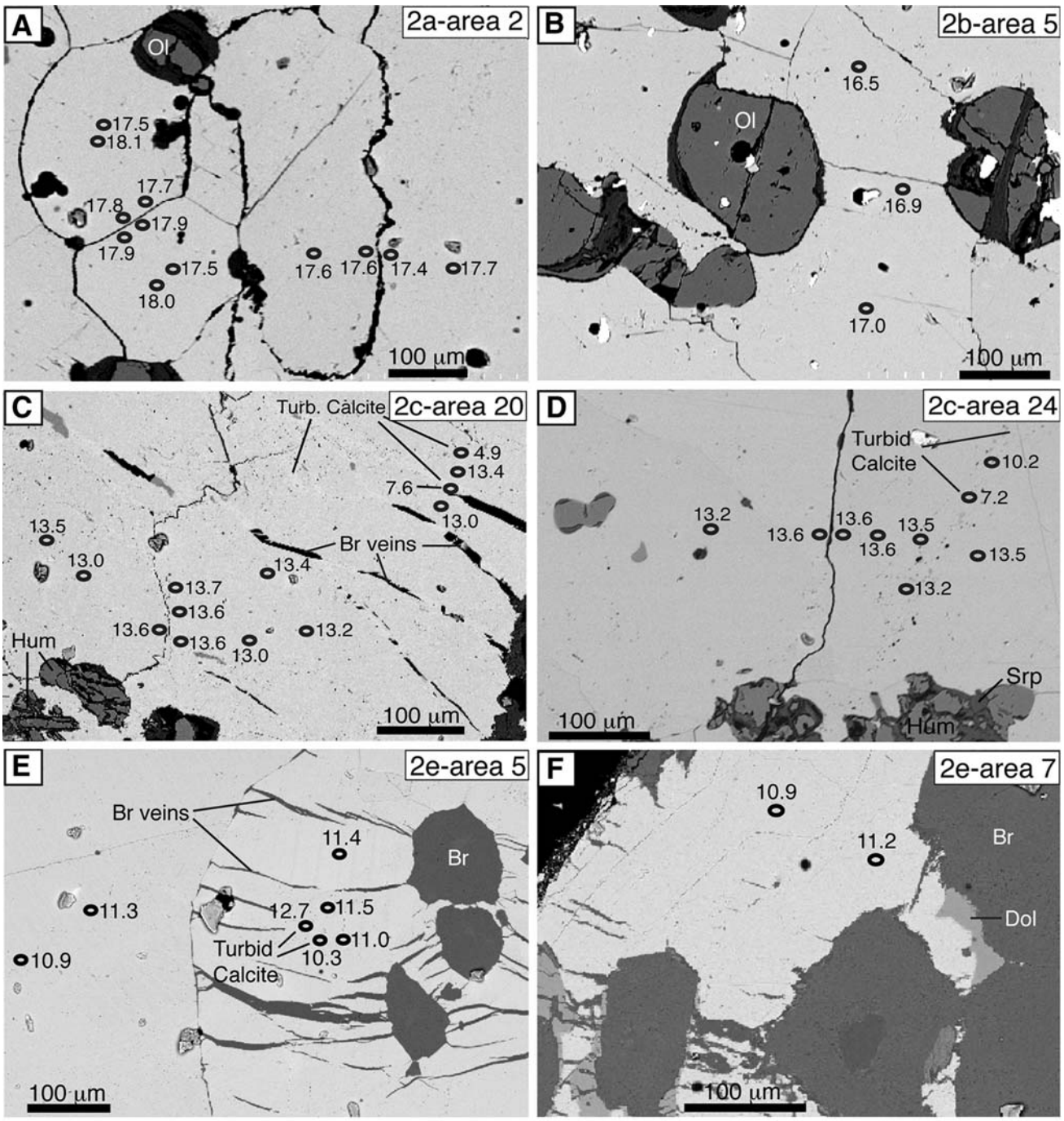

Fig. 8 SEM back-scattered electron (BSE) images of calcite marbles from several locations along the traverse across the layer 8/9 boundary at site I, with locations and results of ion microprobe $\delta^{18}O$ analyses superimposed. Locations of mounts shown in Fig. 7. Mineral abbreviations are *Br* brucite, *Dol* dolomite, *Hum* humite, *Ol* olivine, *Srp* serpentine. Mount locations of images are **a** = Mount 2a, area 2; **b** = Mount 2b, area 5; **c** = Mount 2c, area 20; **d** = Mount 2c, area 24; **e** = Mount 2e, area 5; **f** = Mount 2e, area 7. These images, along with those from areas 4 and 8 from mount 2d (**b** and **c,** Fig. 5), illustrate the common situation where individual clear calcite grains throughout the $\delta^{18}O$ profile at the 8/9 boundary, both within the $\delta^{18}O$ gradient and within the interiors of layers 8 and 9, are homogeneous in $\delta^{18}O$ within analytical uncertainty (±0.27‰, 2SD). Images **c** and **d** in this figure also show the development of 'turbid' (retrograde), low $\delta^{18}O$ calcite along microfractures within calcite grains (see also Fig. 5). Image **e** illustrates a rare example of high $\delta^{18}O$ 'turbid' calcite adjacent to the end of a brucite-filled fracture within an otherwise clear calcite grain (see text for discussion)

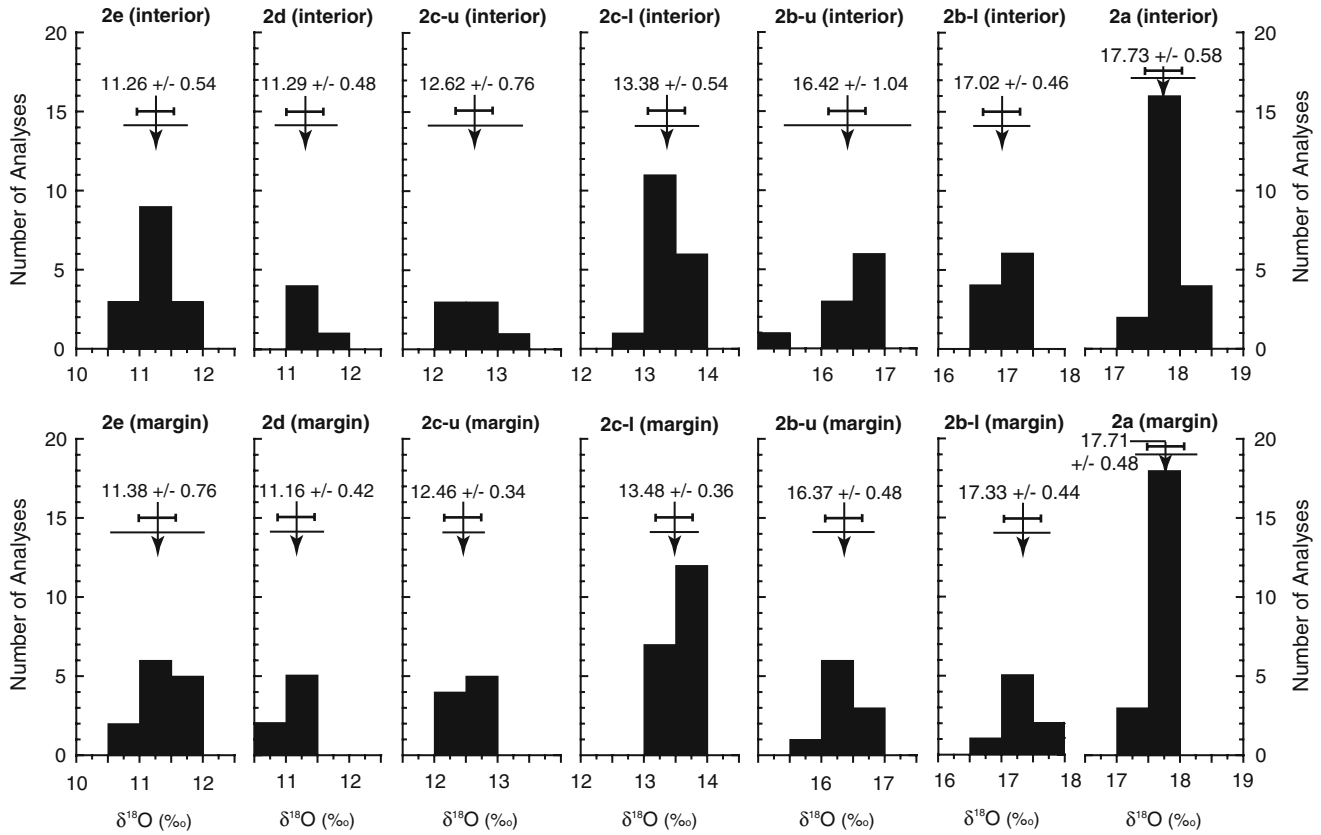

Fig. 9 Composite of histogram plots comparing 174 ion microprobe $\delta^{18}O$ values for grain interiors and margins of clear calcite from the five polished mounts (2a to 2e) across the layer 8/9 boundary. An analysis was defined as interior if the spot was located within the inner two-thirds of the grain radius; as margin if the spot was located in the outer one-third of the grain radius. As a result, grain interiors and margins refer approximately to the inner and outer halves by volume of the calcite grain. Because mounts 2b and 2c are located within the steep gradient in $\delta^{18}O$ beneath the layer 8/9 boundary, both are divided stratigraphically into *upper* (u) and *lower* (l) halves to minimize the impact of the oxygen isotopic gradient across this interval on the comparison of the standard deviation of the data set to the analytical uncertainty for individual analyses. Mean $\delta^{18}O$ values and standard deviation (2SD) of the analyses are given for each histogram. The standard deviation (2SD) of the data is also shown by the *thin horizontal line*. The typical analytical uncertainty of the ion microprobe measurements of $\delta^{18}O$ in the standard calcite UWC-1 ($\pm$0.27, 2SD) is shown by the *heavy horizontal lines* (*with bars*) above. The histograms show that there is very little systematic difference in the $\delta^{18}O$ values of grain interiors and margins at any given location within the traverse; that is, calcite grains are typically homogeneous in their $\delta^{18}O$ values, within analytical uncertainty, even within the steep $\delta^{18}O$ gradient

the steep gradient in $\delta^{18}O$. Hence, the $\delta^{18}O$ gradient across any single calcite grain within the larger-scale $\delta^{18}O$ gradient will typically be 0.08‰, well within analytical uncertainty of the ion probe measurements.

Discussion

Layers 8 and 9 in traverse I of the periclase zone of the Alta aureole have experienced significant but differential $^{18}O/^{16}O$ depletion relative to original protolith values during contact metamorphism. These significant $^{18}O/^{16}O$ depletions require both layers to have exchanged pervasively with significant fluxes of low $\delta^{18}O$ fluids that infiltrated through both layers, but layer 9 must have exchanged with higher fluid fluxes to account for its lower $\delta^{18}O$ value (10.8‰). In addition, calcite preserved a coherent gradient in $\delta^{18}O$ from 17.5 to 10.8‰ in the uppermost 8 cm of layer 8 at the boundary between layers 8 and 9. This gradient is shown by both drill sample and in situ ion microprobe analyses. The progressive depletion in $^{18}O/^{16}O$ in the uppermost 8 cm of layer 8 to $\delta^{18}O$ values of 10.8‰ requires calcite at the top of layer 8 to experience additional infiltration of a lower $\delta^{18}O$ fluid and further isotopic exchange with this fluid. As the uppermost part of layer 8 has a $\delta^{18}O$ value equal to that of layer 9, the most straightforward interpretation is that this lower $\delta^{18}O$ fluid infiltrated layer 8 from layer 9, regardless of the geometric details of this flow. Hence, the $\delta^{18}O$ gradient likely resulted from advective transport of an initial discontinuity in $\delta^{18}O$ developed at the layer 8/9 boundary a short distance ($\sim$4 cm) into the higher $\delta^{18}O$ layer 8, and broadening of this discontinuity by

diffusion and/or dispersion. Infiltration of $^{18}O/^{16}O$-depleted (HF-bearing) fluids from the humite-bearing layer 9 is also supported by replacement of olivine by fluorine-rich humite minerals in the upper 3 cm of layer 8.

Despite significant and pervasive depletion of $^{18}O/^{16}O$ in calcite throughout both layers, ion microprobe analyses indicate that unaltered (clear) calcite grains are now internally homogeneous in $\delta^{18}O$ within analytical uncertainty (±0.27‰, 2SD) across this entire 8/9 boundary profile, including the top 8 cm of layer 8 containing the steep $\delta^{18}O$ gradient. However at some point, and for some time period during this process of exchange, individual calcite grains would have been zoned isotopically, either continuously if diffusion was the dominant mechanism of exchange or discontinuously if a surface reaction mechanism was dominant, or some combination of the two if both mechanisms were important (Fig. 1).

Two important questions therefore are; when were the calcite grains homogenized isotopically and what mechanisms produced this homogenization? Calcite grains could have been homogenized during the initial $^{18}O/^{16}O$ depletion in layers 8 and 9 and advance of the 8/9 boundary gradient into layer 8 that accompany the prograde development of the periclase zone (metamorphism) or later, during the initial stages of cooling of this portion of the periclase zone (retrograde alteration). Calcite grains could have homogenized isotopically by surface reaction mechanisms accompanying recrystallization (relatively rapid) or by volume diffusion (more slowly)—or combination of both.

It is possible to test whether or not calcite cores could have achieved—or closely approximated—exchange equilibrium by volume diffusion with the infiltrating fluid during the prograde segment of contact metamorphism. The time window available for the prograde development of the $\delta^{18}O$ gradient at the 8/9 boundary would correspond to the time required for the periclase reaction front (isograd) to advance from the location of Traverse I (when the isotopic discontinuity at the layer 8/9 boundary would be developed initially) to its observed maximum distance from the igneous contact, 200 m. Cook et al. (1997) estimated a ~5,000 year timescale for the advance of the periclase front to this maximum distance. This timescale is based on heat and mass transport modeling of infiltration-driven metamorphism in the Alta aureole, constrained by calcite-dolomite geothermometry and the observed extent of $^{18}O/^{16}O$ depletion in marbles of the aureole. Assuming for simplicity a constant rate of advance, the periclase front would advance from the location of Traverse I (150 m from the igneous contact) to its observed maximum distance of 200 m in about 1,250 years. During this ~1,250 year time span available for the prograde development of the $\delta^{18}O$ profile at the layer 8/9 boundary, temperature remained within the range of 575 to 600°C.

An estimate of the time necessary to exchange isotopically the interior of a calcite grain is relatively straightforward to calculate for the case of isothermal annealing. The mathematics of non-steady state diffusion (Crank 1975) can be used to compute the time necessary to achieve a certain amount of oxygen isotope exchange at a grain center under isothermal conditions, assuming that grain boundaries are continuously wet by infiltrating fluids. This time estimate is a function of the diffusivity (D) of oxygen in calcite, grain size and grain shape. For modeling, we assume the calcite grains have spherical geometry and that there are no fast-pathways of exchange within grains. Analytical solutions are available to compute the required time for a given amount of change in $\delta^{18}O$ value at the grain center with the simplifying conditions of uniform initial $\delta^{18}O$ value of the grain interior and a fixed grain boundary $\delta^{18}O$ value over time (equations 6.18, 6.19, p. 91, Crank, 1975). The initial $\delta^{18}O$ value of the grain interior is set at 17.2‰, the value of the higher $\delta^{18}O$ layer 9. The grain boundary $\delta^{18}O$ value is fixed at 11.8‰, corresponding to the $\delta^{18}O$ value of layer 9, the local source of fluids infiltrating layer 8. For the same short dimension, spherical geometry requires shorter times for a given amount of exchange at a grain center than do other grain geometries (cube, cylinder, sheet), and hence produces the minimum estimate of the required time.

Watson and Cherniak (1997) use this non-steady state diffusion approach to develop 'center-preservation' criteria for original $\delta^{18}O$ values of zircon grain centers in isothermal annealing scenarios. For example, the center of a sphere will retain its original $\delta^{18}O$ value for times corresponding to values of Dt/a^2 (dimensionless time) up to 0.03, where D is the diffusivity of oxygen in calcite (cm^2/s), t is time (s), and a is grain radius (cm) (Fig. 10). Similarly, the center of a spherical grain will achieve 90% exchange—and be effectively re-equilibrated—for times corresponding to values of $Dt/a^2 = 0.3$ (Crank 1975) (Fig. 10). For the 6.4‰ difference in $\delta^{18}O$ value between layers 8 and 9, 90% exchange at the centers of calcite grains in the uppermost part of layer 8 would yield a difference between center and rim of 0.64‰. In comparison, the average $\delta^{18}O$ values of grain interiors and margins at all five locations along the boundary traverse differ by at most 0.31‰ (Fig. 9), a difference that is also well within the analytical uncertainty (±0.27, 2SD) for the bulk of the ion microprobe analyses (see eTable 1 of Electronic Supplementary Material). Hence most grains are isotopically homogeneous within analytical uncertainty. The maximum difference in $\delta^{18}O$ allowed by analytical uncertainty, 0.54‰, would correspond to 91.5% exchange at grain centers. Therefore, 90% is a conservative estimate of the exchange experienced by the calcite grain interiors. The difference allowed currently by analytical uncertainty, 0.54‰, could be resolved further with multiple analyses of

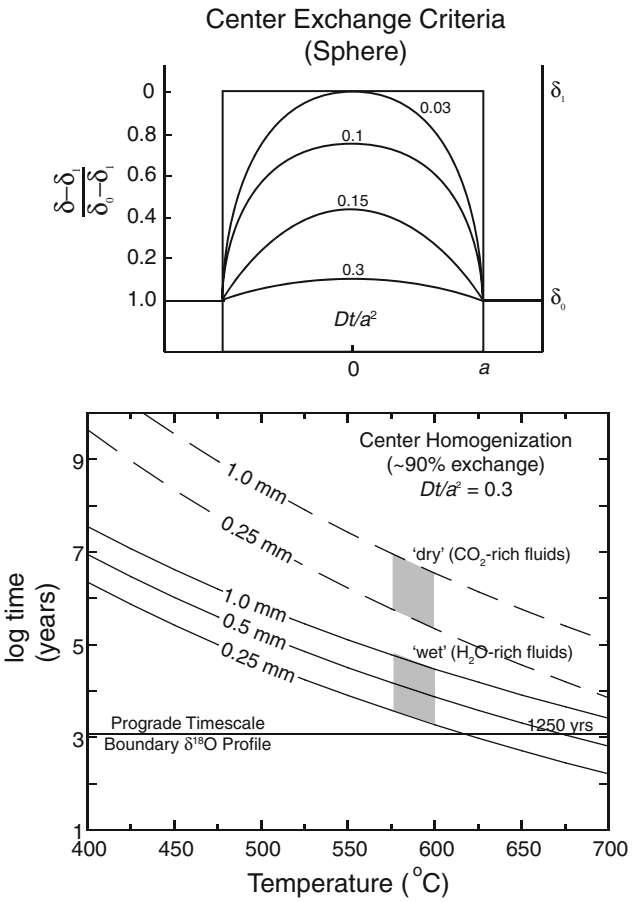

Fig. 10 *Above*: Concentration-distance profiles (schematic) for different times resulting from diffusion in a sphere of radius a with initial concentration within the sphere δ_1 and fixed surface concentration δ_0. Curves are labeled with values of dimensionless time tau (τ), $\tau = Dt/a^2$, where D is diffusivity of oxygen in calcite (cm^2/s) and t is time (s). Grain centers will retain original concentration for values of tau up to 0.03. Grain centers will become effectively equilibrated (>90% exchanged) within analytical uncertainty (±0.27, 2SD) at values of $\tau \geq 0.3$. *Below*: Time-temperature-grain size criteria for center homogenization of oxygen isotopes by diffusion during isothermal annealing of calcite grains. The curves define the times necessary for 90% exchange of oxygen isotopes in the center of calcite grains as a function of temperature and grain size (radius); see text for details. *Solid curves* utilize the diffusivity data for oxygen from Farver (1994) for 'wet' conditions (H_2O-rich fluids); the dashed curves the diffusivity data for oxygen from Labotka et al. (2004) for 'dry' conditions (CO_2). The areas marked in gray denote that range of times necessary for center homogenization by 'wet' and 'dry' diffusion for the range in T (575–600°C) defined for the periclase-forming reaction (Cook and Bowman 1994) and the range in size (radius) for the bulk of calcite grains in the marble. The line drawn at 1,250 years marks the likely upper limit to the timescale for development of the $\delta^{18}O$ profile at the layer 8/9 boundary during prograde metamorphism (see text for details)

the cores and rims of individual calcite grains in future studies.

Figure 10 illustrates temperature (T)–time windows necessary to produce 90% exchange at grain centers ($Dt/a^2 = 0.3$)—effective center homogenization—as functions of temperature and grain radius. Calcite–dolomite geothermometry defines temperatures of 575–600°C for the outer periclase zone in the Alta aureole (Cook and Bowman 1994). Grain sizes of calcite in layers 8 and 9 typically range from 0.25 to 1.0 mm in radius. T–time curves are illustrated in Fig. 10 for grain radii of 0.25, 0.5 and 1.0 mm using the diffusivity data measured at 'wet' conditions (solid lines, water-rich fluids) from Farver (1994) and for 0.25 and 1.0 mm using the diffusivity data measured at 'dry' conditions (dashed lines, CO_2) from Labotka et al. (2004). Gray boxes define required ranges in time for 90% isotopic exchange (~center homogenization) at grain centers for the permitted ranges in T and grain size using the two different values for the diffusivity. The faster diffusivity values from Farver (1994) are likely more relevant to the prograde development of the periclase zone in the Alta aureole, which involved infiltration of water-rich fluids. Even these faster diffusivity values require at least 2,000–62,000 years (lower gray box, Fig. 10) for the centers of calcite grains with radii from 0.25 to 1.0 mm radius to become 90% exchanged by diffusion at a temperature between 575 and 600°C. These time periods are 2× to 50× longer than the estimated time frame of 1,250 years available for prograde development of the oxygen isotope profile at the 8/9 boundary. As analyzed grains with radius up to 1.0 mm are isotopically homogeneous, the minimum time scales necessary for isotopic homogenization by volume diffusion at 575 to 600°C are more realistically 62,000 to ~30,000 years (Fig. 10). These calculations indicate that it is very unlikely that the calcite grains within this profile could have been homogenized isotopically by diffusion during the prograde development of the periclase zone. It is even more unlikely that diffusive homogenization would occur at the lower temperatures of retrograde metamorphism. At 500°C, isotopic homogenization of the centers of calcite grains ranging from 0.25 to 1.0 mm radius would require from 41,500 to 665,000 years (Fig. 10). In comparison, numerical modeling of heat and mass transport in the periclase zone (Cook et al. 1997) predicts that Traverse I would cool to below 500°C within ~20,000 years following maximum advance of the periclase isograd.

The ion microprobe data and these diffusion calculations suggest instead that surface reaction mechanisms (dissolution–reprecipitation) accompanying recrystallization are responsible for the observed oxygen isotope homogeneity of calcite in the periclase zone of the Alta aureole. Replacement textures described by Putnis (2002) in natural systems and in experiments on replacement reactions involving simple salts provide some insights into the processes responsible for isotopic homogenization in the Alta calcites. Putnis (2002) interprets these textures to indicate that mineral replacement reactions result primarily from

dissolution–reprecipitation processes. The initial stage of replacement typically involves replacement of grain margins—the development of replacement rims. Replacement involving chemical/isotopic exchange can produce an exchanged, replacement rim in structural continuity with the parent grain; continued reaction eventually replaces the initial grain with a single, replaced grain such as observed in the periclase zone calcites at Alta. Recent experiments on the recrystallization of quartzite in the presence of a SiO_2-saturated fluid phase by Nakamura and Watson (2001) demonstrate that replacement reactions may be driven by the relatively small free energy reduction accompanying grain size increase associated with recrystallization. Textures reported by Putnis (2002) indicate that the replacement reaction is often accompanied by significant increase in porosity in the replacement product phase. This transitory increase in porosity allows access of fluid to the replacement front so that the front can advance into the interior of grains to complete the replacement of the grain. Although the turbid calcite replacing clear calcite at Traverse I exhibits noticeable microporosity, clear calcite does not. However, the experiments of Putnis (2002) also show that the porous replacement domain evolves to a lower porosity state with time as the microporosity is filled by continued epitaxial growth of the replacement product phase. The isotopically homogeneous clear calcite at Traverse I may record this stage of evolution.

The ion microprobe data do not resolve whether recrystallization and isotopic homogenization took place during the prograde development of the periclase zone or during early stages of retrograde cooling. Surface reaction processes leading to isotopic exchange in calcite might be expected to be relatively rapid at temperatures at or near those of the periclase isograd (575–600°C) from available experimental data (Cole 1992; Cole and Chakraborty 2001). Thermal modeling results indicate that temperatures would remain in excess of 550°C for ~8,000 years after cessation of the main phase of layer-parallel fluid flow associated with prograde development of the periclase zone (Cook et al., 1997). Thus there would appear to be ample time during both prograde and retrograde metamorphism for grain scale homogenization through recrystallization, assuming the experimental data are applicable to the physico-chemical conditions accompanying prograde and retrograde development of the periclase zone in the Alta aureole.

Calcite-dolomite geothermometry results in the periclase zone (Cook and Bowman 1994) may provide some additional insight. Maximum calcite-dolomite temperatures recorded in a number of samples from the inner periclase zone are in the range of 500–550°C rather than the peak temperatures of 575–625°C. These low temperatures indicate that some calcite within the periclase zone has experienced significant retrograde exchange of Mg content. The diffusivity of Mg in calcite has been measured at 'dry' (CO_2) conditions (Fisler and Cygan 1999). These results indicate that the diffusion of Mg is approximately 10× faster than the diffusion of oxygen in calcite under dry conditions and at least 10× slower than the diffusion of oxygen in calcite under wet conditions, in the temperature range 500 to 600°C. The diffusivity of Mg in calcite under wet conditions has not been measured. Existing experimental studies (summarized in Watson and Baxter 2007, p. 319) suggest that elevated water pressures do not enhance significantly the diffusivity of cations in minerals such as calcite (C), zircon (Pb, Ti), plagioclase (Sr), and apatite (Sr) at crustal P–T conditions. If the experimental D_{Mg} (dry) diffusivity data are applicable to the water-rich conditions of the Alta periclase zone, calculations analogous to those for oxygen isotopes, for the same range of temperature and grain size, indicate that 90% center homogenization of Mg content in calcite by diffusion would require time periods of 100,000 to 5.4 million years. These time periods are much longer than the estimated time periods for either prograde development of the entire periclase zone (~5000 years) or for cooling of the outer periclase zone to below 500°C (~20,000 years) (Cook et al. 1997). Provided the diffusivity of Mg in calcite is not enhanced significantly under wet conditions (e.g., at elevated water pressure), it is unlikely that volume diffusion of Mg is responsible for the retrograde exchange of Mg in the calcite. Alternatively, these calculations suggest that recrystallization is the mechanism responsible for retrograde exchange of Mg in calcite. Retrograde recrystallization of calcite in the temperature range 500–550°C may also be responsible for part of the oxygen isotope homogenization of calcite.

Conclusions

Ion microprobe analyses have been made on calcite along a traverse across two layers in the periclase zone of the Alta aureole that have experienced significant, but different degrees of $^{18}O/^{16}O$ depletion during their prograde metamorphic development. The ion microprobe analyses indicate that unaltered (clear) calcite grains are now internally homogeneous in $\delta^{18}O$ within analytical uncertainty (±0.27‰, 2SD) across this entire traverse (the boundary between layers 8 and 9 at traverse I), including the top 8 cm of layer 8 containing the steep $\delta^{18}O$ gradient. Simple diffusion calculations indicate that the calcite grains along this traverse cannot have homogenized by volume diffusion during the development of the oxygen isotope profile at the layer 8/9 boundary that accompanies the prograde development of the periclase zone. Nor is it likely that the calcite grains homogenized by volume

diffusion during retrograde cooling of the inner aureole. Instead, isotopic homogenization likely resulted from recrystallization. The ion microprobe data are consistent with the formation of calcite in oxygen isotope exchange equilibrium with infiltrating fluid during prograde reaction and recrystallization. However, the presence of retrograde calcite-dolomite temperatures recorded in calcite from the periclase zone suggests that both Mg exchange and oxygen isotope homogenization also accompanied recrystallization during the early stages of retrograde cooling. Thus recrystallization has been effective in homogenizing the oxygen isotope compositions of calcite at the grain scale within the relatively short time period available for contact metamorphism and initial cooling in the Alta aureole.

Acknowledgments National Science Foundation (NSF) Grant #EAR05-09639 and Department of Energy Grant #93ER14389 to J. W. V. and Petroleum Research Fund Grant # 43498-AC8 to J. R. B. are gratefully acknowledged. The Wisc-SIMS Ion Microprobe lab is partly supported by NSF Grants #EAR-0319230 and 0516725, and the University of Wisconsin, Department of Geology and Geophysics Weeks Fund. John Fournelle provided significant assistance with SEM imaging.

References

Abart R, Sperb R (1997) Grain-scale stable isotope disequilibrium during fluid-rock interaction. 1: Series approximations for advective-dispersive transport and first-order kinetic mineral-fluid exchange. Am J Sci 297:679–706

Ague JJ, Rye DM (1999) Simple models of CO_2 release from metacarbonates with implications for interpretation of directions and magnitudes of fluid flow in the deep crust. J Petrol 40:1443–1462. doi:10.1093/petrology/40.9.1443

Arita Y, Wada H (1990) Stable isotope evidence for migration of metamorphic fluids along grain boundaries of marbles. Geochem J 24:173–186

Baker AA, Calkins FC, Crittenden MD, Bromfield CS (1966) Geologic map of the Brighton quadrangle, Utah. U.S. Geological Survey Map GQ–535

Baumgartner LP, Valley JW (2001) Stable isotope transport and contact metamorphic fluid flow. In: Valley JW, Cole DR (eds) Stable isotope geochemistry. Reviews in mineralogy and geochemistry, vol 43. Mineralogical Soceity of America, Washington, DC, pp 415–468

Bickle MJ, Baker J (1990a) Advective-diffusive transport of isotopic fronts—an example from Naxos, Greece. Earth Planet Sci Lett 97:78–97. doi:10.1016/0012-821X(90)90100-C

Bickle MJ, Baker J (1990b) Migration of reaction and isotopic fronts in infiltration zones: assessments of fluid flux in metamorphic terrains. Earth Planet Sci Lett 98:1–13. doi:10.1016/0012-821X(90)90083-A

Bickle MJ, Chapman HJ, Ferry JM, Rumble D, Fallick AE (1997) Fluid flow and diffusion in the Waterville limestone, south-central Maine: constraints from strontium, oxygen, and carbon isotope profiles. J Petrol 38:1489–1512. doi:10.1093/petrology/38.11.1489

Blattner P, Lassey KR (1989) Stable-isotope exchange fronts, Damkohler numbers, and fluid to rock ratios. Chem Geol 78:381–392. doi:10.1016/0009-2541(89)90070-3

Bolton EW, Rye DM, Ague JJ, Luttge A (2004) Modeling contact metamorphism of siliceous dolomite via kinetic control of overall reactions. In: Wanty RB, Seal II RR (eds) Proceedings of the 11th International symposium on water–rock interaction, vol 1. Routledge, UK, pp 269–272

Bowman JR, Willett SD (1991) Spatial patterns of oxygen isotope exchange during one-dimensional fluid infiltration. Geophys Res Lett 18:971–974. doi:10.1029/91GL01079

Bowman JR, Willett SD, Cook SJ (1994) Oxygen isotopic transport and exchange during fluid flow: one-dimensional models and applications. Am J Sci 294:1–55

Cole DR (1992) Influence of solution composition and pressure on the rates of oxygen isotope exchange in the system calcite–H_2O–NaCl at elevated temperatures. Chem Geol 102:199–216. doi:10.1016/0009-2541(92)90156-Y

Cole DR, Chakraborty S (2001) Rates and mechanisms of isotopic exchange. In: Valley JW, Cole DR (eds) Stable isotope geochemistry, reviews in mineralogy and geochemistry, vol 43. Mineralogical Soceity of America, Washington, DC, pp 83–224

Cole DR, Larson PB, Riciputi LR, Mora CI (2004) Oxygen isotope zoning profiles in hydrothermally altered feldspars: estimating the duration of water–rock interaction. Geology 32:29–32. doi:10.1130/G19881.1

Cook SJ (1992) Contact Metamorphism Surrounding the Alta Stock, Little Cottonwood Canyon, Utah. Ph.D. thesis. University of Utah, Salt Lake City

Cook SJ, Bowman JR (1994) Contact metamorphism surrounding the Alta stock: thermal constraints and evidence of advective heat transport from calcite–dolomite geothermometry. Am Mineral 79:513–525

Cook SJ, Bowman JR (2000) Mineralogical evidence for fluid-rock interaction accompanying prograde contact metamorphism of siliceous dolomites: Alta Stock Aureole, Utah, USA. J Petrol 41:739–757. doi:10.1093/petrology/41.6.739

Cook SJ, Bowman JR, Forster CB (1997) Contact metamorphism surrounding the Alta Stock: finite element model simulation of heat- and $^{18}O/^{16}O$ mass-transport during prograde metamorphism. Am J Sci 297:1–55

Crank J (1975) The mathematics of diffusion, 2nd edn. Oxford University Press, London, p 414

Crittenden MD, Stuckless JS Jr, Kistler RW, Stern TW (1973) Radiometric dating of intrusive rocks in the Cottonwood area, Utah. U S Geol Surv J Res 1:173–178

Cui X, Nabelek PI, Liu M (2002) Numerical modeling of fluid flow and oxygen isotope exchange in the Notch Peak contact metamorphic aureole, Utah. Geol Soc Am Bull 114:869–882. doi 10.1130/0016-7606(2002)114<0869:NMOFFA>2.0.CO;2

Cui X, Nabelek PI, Liu M (2003) Reactive flow of mixed CO_2–H_2O fluid and progress of calc-silicate reactions in contact metamorphic aureoles: insights from two-dimensional numerical modeling. J Metamorph Geol 21:663–684. doi:10.1046/j.1525-1314.2003.00475.x

Eppel H, Abart R (1997) Grain-scale stable isotope disequilibrium during fluid-rock interaction. 2: An example from the Penninic-Austroalpine tectonic contact in eastern Switzerland. Am J Sci 297:707–728

Farver JR (1994) Oxygen self-diffusion in calcite: dependence on temperature and water fugacity. Earth Planet Sci Lett 121:575–587

Ferry JM, Wing BA, Rumble DIII (2001) Formation of wollastonite by chemically reactive fluid flow during contact metamorphism, Mt. Morrison Pendant, Sierra Nevada, California, USA. J Petrol 42:1705–1728. doi:10.1093/petrology/42.9.1705

Fisler DK, Cygan RT (1999) Diffusion of Ca and Mg in calcite. Am Mineral 84:1392–1399

Ganor J, Matthews A, Paldor N (1989) Constraints on effective diffusivity during oxygen isotope exchange at a marble-schist contact, Sifnos (Cyclades), Greece. Earth Planet Sci Lett 94:208–216. doi:10.1016/0012-821X(89)90140-4

Graham CM, Valley JW, Eiler JM, Wada H (1998) Timescales and mechanisms of fluid infiltration in a marble: an ion microprobe study. Contrib Mineral Petrol 132:371–389. doi:10.1007/s004100050430

Gerdes ML, Valley JW (1994) Fluid flow and mass transport at the Valentine Wollastonite deposit, Adirondack Mountains. N Y J Metamorph Geol 12:589–608. doi:10.1111/j.1525-1314.1994.tb00045.x

Gerdes ML, Baumgartner LP, Person M, Rumble DIII (1995) One- and two-dimensional models of fluid flow and stable isotope exchange at an outcrop in the Adamello contact aureole, Southern Alps, Italy. Am Mineral 80:1004–1019

Kita NT, Ikeda Y, Togashi S, Liu YZ, Morishita Y, Weisberg MK (2004) Origin of ureilites inferred from a SIMS oxygen isotopic and trace element study of clasts in the Dar al Gani 319 polymict ureilite. Geochim Cosmochim Acta 68:4213–4235. doi:10.1016/j.gca.2004.03.020

Kita NT, Ushikubo T, Fu B, Spicuzza MJ, Valley JW (2007) Analytical developments on oxygen three isotope analyses using a new generation ion microprobe IMS-1280. Lunar Planet Sci Conf. 38, Abstr. #1981

Labotka TC, Cole DR, Riciputi LR, Fayek M (2004) Diffusion of C and O in calcite from 0.1 to 200 MPa. Am Mineral 89:799–806

Lackey JS, Valley JW (2004) Complex patterns of fluid flow during wollastonite formation in calcareous sandstones at Laurel Mountain, Mt. Morrison Pendant, California. Geol Soc Am Bull 116:76–93

Lasaga AC, Rye DM (1993) Fluid flow and chemical reaction kinetics in metamorphic systems. Am J Sci 293:361–404

Lasaga AC, Rye DM, Luettge A, Bolton EW (2000) Dynamic treatment of invariant and univariant reactions in metamorphic systems. Am J Sci 300:173–221. doi:10.2475/ajs.300.3.173

Lasaga AC, Rye DM, Luettge A, Bolton EW (2001) Calculation of fluid fluxes in Earth's crust. Geochim Cosmochim Acta 65:1161–1185. doi:10.1016/S0016-7037(00)00545-7

Lassey KR, Blattner P (1988) Kinetically controlled oxygen isotope exchange between fluid and rock in one-dimensional advective flow. Geochim Cosmochim Acta 52:2169–2175. doi:10.1016/0016-7037(88)90197-4

Lewis S, Holness M, Graham CM (1998) Ion microprobe study of marble from Naxos, Greece: grain-scale fluid pathways and stable isotope equilibration during metamorphism. Geology 26:935–938. doi 10.1130/0091-7613(1998)026<0935:IMSOMF>2.3.CO;2

Luttge A, Bolton EW, Rye DM (2004) A kinetic model of metamorphism: an application to siliceous dolomites. Contrib Mineral Petrol 146:546–565. doi:10.1007/s00410-003-0520-8

Matthews A, Lieberman J, Avigad D, Garfunkel Z (1999) Fluid–rock interaction and thermal evolution during thrusting of an Alpine metamorphic complex (Tinos Island, Greece). Contrib Mineral Petrol 135:212–224. doi:10.1007/s004100050507

McCrea JM (1950) The isotope chemistry of carbonates and a paleotemperature scale. J Chem Phys 18:849–857. doi:10.1063/1.1747785

Moore JN, Kerrick DM (1976) Equilibria in siliceous dolomites of the Alta aureole, Utah. Am J Sci 276:502–524

Muller T, Baumgartner LP, Foster CT, Vennemann TW (2004) Metastable mineral growth in contact aureoles. Geology 32:821–824. doi:10.1130/G20576.1

Nakamura M, Watson EB (2001) Experimental study of aqueous fluid infiltration into quartzite: implications for the kinetics of fluid redistribution and grain growth driven by interfacial energy reduction. Geofluids 1:73–89. doi:10.1046/j.1468-8123.2001.00007.x

Page FZ, Ushikubo T, Kita NT, Riciputi LR, Valley JW (2007) High precision oxygen isotope analysis of picogram samples reveals 2-μm gradients and slow diffusion in zircon. Am Mineral 92:1772–1775. doi:10.2138/am.2007.2697

Pollington AD, Bowman JR, Kaszuba JP (2005) Heterogeneous fluid flow, reaction progress, and isotope disequilibrium in the talc zone, outer Alta aureole, Utah (abst): Geol. Soc. Amer. Mtg., Salt Lake City, UT

Putnis A (2002) Mineral replacement reactions: from macroscopic observations to microscopic mechanisms. Miner Mag 66:689–708. doi:10.1180/0026461026650056

Roselle GT, Baumgartner LP, Valley JW (1999) Stable isotope evidence of heterogeneous fluid infiltration at the Ubehebe Peak contact aureole, Death Valley National Park, California. Am J Sci 299:93–138

Valley JW (1986) Stable isotope geochemistry of metamorphic rocks. In: Valley JW, Taylor HP, O'Neil JR (eds) Stable isotopes in high temperature geological processes. Reviews in mineralogy, vol 16. Mineralogical Soceity of America, Washington, DC, pp 445–490

Valley JW (2001) Stable isotope thermometry at high temperatures: In: Valley JW, Cole DR (eds) Stable isotope geochemistry. Reviews in mineralogy and geochemistry, vol. 43, p. 365–414

Valley JW, Graham CM (1996) Ion microprobe analysis of oxygen isotope ratios in quartz from Skye granite: healed micro-cracks, fluid flow, and hydro-thermal exchange. Contrib Mineral Petrol 124(3/4):225–234. doi:10.1007/s004100050188

Wada H (1988) Microscale isotopic zoning in calcite and graphite crystals in marble. Nature 331:61–63. doi:10.1038/331061a0

Watson EB, Cherniak DJ (1997) Oxygen diffusion in zircon. Earth Planet Sci Lett 148:527–544. doi:10.1016/S0012-821X(97)00057-5

Watson EB, Baxter EF (2007) Diffusion in solid-earth systems. Earth Planet Sci Lett 253:307–327. doi:10.1016/j.epsl.2006.11.015

Wilson JW (1961) Geology of the Alta stock. Ph.D. thesis, California Institute of Technology, Pasadena

Yardley BWD, Lloyd GE (1995) Why metasomatic fronts are really metasomatic sides. Geology 23:53–56. doi 10.1130/0091-7613(1995)023<0053:WMFARM>2.3.CO;2